Studying plasmonic resonance modes of hierarchical self-assembled meta-atoms based on their transfer matrix

Radius N. S. Suryadharma,[1,*] Martin Fruhnert,[1] Ivan Fernandez-Corbaton,[2] and Carsten Rockstuhl[1,2]
[1]*Institute of Theoretical Solid State Physics, Karlsruhe Institute of Technology, Wolfgang-Gaede-Strasse 1, 76131 Karlsruhe, Germany*
[2]*Institute of Nanotechnology, Karlsruhe Institute of Technology, P.O. Box 3640, 76021 Karlsruhe, Germany*
(Received 2 November 2016; revised manuscript received 30 May 2017; published 7 July 2017)

Hierarchical self-assembled meta-atoms are made from a larger number of suitably arranged metallic nanoparticles. They constitute the basic building blocks for isotropic metamaterials. The properties of these meta-atoms are usually studied upon illumination with a plane wave and by analyzing the multipolar composition of the scattered field. This, however, does not always provide full information. The coupling between multiple meta-atoms is usually not considered, and a physical understanding for the cause of the response is often incomplete. Here we overcome these limitations by performing a spectral eigenvalue analysis of the transfer matrix of isolated and coupled self-assembled meta-atoms. Emphasis is put on using a transfer-matrix formulation in either a local or a global coordinate frame. We show that for the magnetic resonance, coupling to nearest neighbors is weak, suggesting the possibility to preserve the response of the isolated meta-atom upon tight packaging in a metamaterial.

DOI: 10.1103/PhysRevB.96.045406

I. INTRODUCTION

With the advent of metamaterials, many unprecedented ways to manipulate the propagation of light came in reach [1–8]. In general, metamaterials are composed of a dense arrangement of basic building blocks. The effective optical response of metamaterials, in lowest order approximation, is derived from the optical response of its individual building blocks. To emphasize this aspect, these building blocks are called meta-atoms [9]. To ease the theoretical analysis, the fabrication, and the characterization of metamaterials, meta-atoms are most frequently periodically arranged [10–13]. However, this causes the effective response of the metamaterials to be affected by effects due to strong spatial dispersion; and the material is usually anisotropic [14–16]. This is a disadvantage for multiple applications envisioned. To mitigate these problems, isotropic self-assembled metamaterials were suggested [17,18]. Many different approaches for their realization have been presented in the past [19–25]. Here we restrict our attention to the broader class of self-assembled metamaterials where the meta-atoms are composed of many metallic nanoparticles [26–30].

The properties of these meta-atoms are usually studied upon illuminating a single meta-atom with a plane wave and by decomposing the scattered field into contributions from different multipole moments [31]. Such analysis, usually, reveals the presence of a strong magnetic dipole moment along with a contribution from an electric dipole moment. Higher order moments are excited as well but very often they can be neglected. Such analysis is insightful; but eventually it is also limited for multiple reasons. Most notably, properties are usually studied at the level of the dispersion in the multipole moments at the isolated particle. This spectral dependence, however, can be quite complicated if multiple resonances contribute to such dispersion. This asks for a deeper physical understanding. Moreover, the magnetic polarizability of most meta-atoms is too weak to allow a sufficiently strong dispersion in the effective permeability in the metamaterial at low filling fractions. Therefore, the meta-atoms have to be densely packed [32]. For a dense arrangement the coupling to nearest neighbors is important, something that is hard to capture using a technique that depends on a specific illumination and that considers only isolated meta-atoms. To study this coupling process requires means of investigation that do not depend on a specific illumination. The property must be attributable to only the meta-atoms, i.e., the hybridization of their individual plasmonic response needs to be studied.

Recently, multiple methods were proposed for this purpose. They shed light on these issues from multiple perspectives. The coupled dipole approximation [33,34] models the particles as dipole (both electric and magnetic) and allows us to study their interaction. As this technique is based on the assumption that each particle's response can be described solely by its dipole moments, the use of this method is limited to subwavelength particles.

Alternatively, the eigenmodes of the meta-atoms can be found. Since the meta-atoms are characterized both by dissipation and strong radiative losses, the scattering operator describing the interaction of light with the meta-atoms is non-Hermitian. This requires the consideration of quasinormal eigenmodes that are linked to poles of the scattering operator in the complex frequency plane [35–38]. Quasinormal eigenmodes are a powerful concept but they also leave a few questions open; especially when applied to problems that live on the real-frequency axis. Also, a local density of states approach [39] has been applied to study the coupling of core-shell systems. But the method suffers from its inability to identify the modes involved in the coupling. Full wave eigenmode analysis based on the volumetric method of moments has been used to predict the line broadening in dolmen structures [40]. Another approach has been using a circuit model to study the coupling of the dolmen structure [41]. Other methods, such as the singularity expansion method have also been proposed to determine the mode amplitude for antenna application [42]. More recently, the spectral analysis of the eigenvalues of the transfer matrix has been proposed to study plasmonic resonances of metallic nanostructures [43]. This

*radius.suryadharma@kit.edu

method, in general, seems to be suitable for our purposes, since the transfer matrix contains all the information of how a given object interacts with an arbitrary illumination at a given real-valued frequency. It can also provide information about the hybridization and the interaction among coupled objects.

Motivated by these developments, we study here plasmonic resonances of self-assembled meta-atoms by diagonalizing the respective transfer matrix. The considered meta-atoms are made from metallic nanoparticles and they shall possess an increasing complexity. This eigenvalue analysis allows us to study the hybridization of modes among coupled meta-atoms. This makes it comparable to hybridization theory but it has the advantage of not being limited to the quasistatic approximation. This eigenvalue analysis can be linked to the scattering and absorption spectra for a given illumination by solving additionally the eigenvalue of the transpose conjugate transfer matrix and by applying suitable bi-orthogonality relations [43]. We show that a spectral decomposition of the eigenvalues into individual resonances with a Lorentzian shape allows for insights into the physical effects that govern the meta-atom response.

We emphasize the possibility to formulate the transfer matrix in a global coordinate system. This will be called the T matrix. It expresses the response of the entire meta-atom. Alternatively, it can be also expressed in a local coordinate system. This will be called the $\mathcal{T}$ matrix. It expresses the response of each individual metallic nanoparticle that make up the meta-atom. The combined use of both formulations allows us to explore features that emerge at different length scales of the hierarchical meta-atoms. Whenever we provide a statement that applies to both formulations we will call it the transfer matrix.

To demonstrate the applicability of the method, we start with a basic meta-atom and increase gradually the complexity. We stress that even though we apply the methodology to specific examples, the method is not restricted to those considered geometries. This makes the framework a powerful tool to study the properties of individual and coupled meta-atoms beyond the mere simulation of their optical response upon plane wave illumination.

II. T-MATRIX FORMULATION

The transfer matrix describes how an incident field couples to the scattered field by a given object. It is a quantity unique to the scattering object and does not depend on the illumination. The scattering process can be described in a global coordinate system if the object is considered as an isolated structure. Alternatively, if the object is composed out of multiple elements, a local formulation for the transfer matrix can be considered. Such local $\mathcal{T}$ matrix expresses the optical response of an object to an illumination in terms of the response of its constituents. Below we describe both formulations; starting with the global formulation.

A. Global formulation

When considering meta-atoms that are locally confined in space, the time harmonic electromagnetic fields involved in the scattering process are most frequently expanded into vector spherical harmonics $\mathbf{M}_{mn}(r,\theta,\phi)$ and $\mathbf{N}_{mn}(r,\theta,\phi)$. They express the fields with electric and magnetic parity [44]. Since we are not interested in the internal structure of the field within a meta-atom, i.e., we are only interested in how it is perceived by an external observer, it suffices to expand the incident field as

$$\mathbf{E}_{\text{inc}}(r,\theta,\phi) = \sum_{n=1}^{N}\sum_{m=-n}^{n} p_{nm}\mathbf{N}^{(1)}_{nm}(r,\theta,\phi) + q_{nm}\mathbf{M}^{(1)}_{nm}(r,\theta,\phi) \tag{1}$$

and the field scattered by the meta-atom as

$$\mathbf{E}_{\text{sca}}(r,\theta,\phi) = \sum_{n=1}^{N}\sum_{m=-n}^{n} a_{nm}\mathbf{N}^{(3)}_{nm}(r,\theta,\phi) + b_{nm}\mathbf{M}^{(3)}_{nm}(r,\theta,\phi). \tag{2}$$

p_{nm}, q_{nm}, a_{nm}, and b_{nm} are the corresponding frequency dependent expansion coefficients, n and m denote the quantum numbers of the respective multipoles, and N expresses the maximum multipolar order retained in the expansion. The superscript denotes the choice of spherical Bessel (1) or spherical Hankel (3) functions as the component of the vector spherical harmonics. All quantities are frequency dependent. The expansion is valid within the spatial domain that excludes the scatterer.

The way an object scatters light is entirely described by its corresponding T matrix [45]. It links the incident and scattered field as

$$\begin{pmatrix} T_{11} & T_{12} \\ T_{21} & T_{22} \end{pmatrix}\begin{pmatrix} p \\ q \end{pmatrix} = \begin{pmatrix} a \\ b \end{pmatrix}. \tag{3}$$

The matrix on the left-hand side is the T matrix in a global coordinate system. It transforms the incident field into the scattered field with respect to the entire scatterer. The submatrices T_{11}, T_{12}, T_{21}, and T_{22} express the transformation from electric to electric, from magnetic to electric, from electric to magnetic, and from magnetic to magnetic multipolar contributions, respectively.

The T matrix can be obtained by multiple means. For a general object, it can be reconstructed from the optical response obtained upon illuminating the object with a sequence of specific fields. For example, using plane waves as an illumination, the scattered field expanded into outgoing vector spherical harmonics delivers a column vector of the T matrix [46]. To obtain the scattered field for a given illumination, Maxwell's equations have to be solved with a full-wave solver of preference. For the hierarchical meta-atoms we are interested in, the T matrix can be constructed from the general multiple scattering problem. It will be mentioned further below.

This global T matrix is not unique. Some ambiguities occur when it comes to the proper choice of the coordinate system with respect to which multipole expansion is performed. In general, there is no easy answer concerning the proper choice of this coordinate center, since eventually any given point in space can be chosen. Technically, even a very remote point can serve the purpose. However, the size of the T matrix necessary to express the response will grow quite quickly for an inappropriately chosen coordinate center, i.e., many multipole moments have to be retained in the expansion. Therefore,

in such global formulation the coordinate system should be wisely chosen to retain the least number of multipole moments in the expansion. For the meta-atoms of interest this is usually a high symmetry point.

B. Local formulation

For some of the self-assembled meta-atoms, and especially for the coupled systems we have in mind, such global formulation is not convenient because the response of each individual meta-atom is mixed together in the global coordinate system. From the final considerations written in the previous section, it is obvious that if the studied object is made out of two remotely coupled meta-atoms, the T-matrix method as formulated in a global coordinate system is cumbersome. The larger the separation among the meta-atoms the larger the T matrix and the less accessible will be the description of the response in a physical sound language. Then, a local formulation is much more convenient, where the local transfer matrices of the individual objects are retained.

To sketch the derivation of such a local $\mathcal{T}$-matrix formulation, we write the incident field acting on a scatterer j in a multiscatterer system as the sum of the external incident field and the scattered field from other scatterers [47]. There, the scattered field from scatterer l with respect to scatterer j can be linked by the addition theorem of spherical harmonics [48]:

$$\mathbf{M}^{(1)}_{nm}(\mathbf{r}_j) = \sum_{\nu}^{N} \sum_{\mu=-\nu}^{\nu} A^{\nu\mu}_{nm}(l,j)\mathbf{M}^{(3)}_{\nu\mu}(\mathbf{r}_l) + B^{\nu\mu}_{nm}(l,j)\mathbf{N}^{(3)}_{\nu\mu}(\mathbf{r}_l), \tag{4}$$

$$\mathbf{N}^{(1)}_{nm}(\mathbf{r}_j) = \sum_{\nu}^{N} \sum_{\mu=-\nu}^{\nu} B^{\nu\mu}_{nm}(l,j)\mathbf{M}^{(3)}_{\nu\mu}(\mathbf{r}_l) + A^{\nu\mu}_{nm}(l,j)\mathbf{N}^{(3)}_{\nu\mu}(\mathbf{r}_l), \tag{5}$$

where $A^{\nu\mu}_{nm}$ and $B^{\nu\mu}_{nm}$ denote the translation coefficient of spherical harmonics. Using these translation coefficients, the vector spherical harmonics coefficients of the total incident field due to an external field and the scattered field from other objects can be written as

$$P^{j}_{nm} = p^{j}_{nm} - \sum_{l\neq j}^{J} \sum_{\nu=1}^{N} \sum_{\mu=-\nu}^{\nu} a^{l}_{\nu\mu} A^{nm}_{\nu\mu}(l,j) + b^{l}_{\nu\mu} B^{nm}_{\nu\mu}(l,j), \tag{6}$$

$$Q^{j}_{nm} = q^{j}_{nm} - \sum_{l\neq j}^{J} \sum_{\nu=1}^{N} \sum_{\mu=-\nu}^{\nu} a^{l}_{\nu\mu} B^{nm}_{\nu\mu}(l,j) + b^{l}_{\nu\mu} A^{nm}_{\nu\mu}(l,j), \tag{7}$$

where P^{j}_{nm} and Q^{j}_{nm} are used to expand the total incident field on the scatterer j, and (p^{j}_{nm}, q^{j}_{nm}) and $(a^{l}_{\nu\mu}, b^{l}_{\nu\mu})$ are the expansion coefficients for the external incident field in local coordinate of the scatterer j and the expansion coefficients for the scattered field from particle l, respectively. J is the total number of scatterers. The scattered fields from each scatterer are obtained by solving the self-consistent equations

$$a^{j}_{nm} = \sum_{\alpha=1}^{N} \sum_{\beta=-\alpha}^{\alpha} T^{j,\alpha\beta nm}_{11} P^{j}_{\alpha\beta} + T^{j,\alpha\beta nm}_{12} Q^{j}_{\alpha\beta}, \tag{8}$$

$$b^{j}_{nm} = \sum_{\alpha=1}^{N} \sum_{\beta=-\alpha}^{\alpha} T^{j,\alpha\beta nm}_{21} P^{j}_{\alpha\beta} + T^{j,\alpha\beta nm}_{22} Q^{j}_{\alpha\beta}. \tag{9}$$

The above equations describe the scattering process in each local coordinate system of the scatterers.

This representation has the advantage that it can trace the multipolar moments of each scatterer individually, rather than the "effective" multipolar moments of the structure with respect to the global coordinate system. For a system made from two objects, by combining Eqs. (6)–(9) and writing them in matrix form, the local $\mathcal{T}$ matrix can be exemplarily written as

$$\begin{pmatrix} \mathcal{T}_{11} & \mathcal{T}_{12} & \mathcal{T}_{13} & \mathcal{T}_{14} \\ \mathcal{T}_{21} & \mathcal{T}_{22} & \mathcal{T}_{23} & \mathcal{T}_{24} \\ \mathcal{T}_{31} & \mathcal{T}_{32} & \mathcal{T}_{33} & \mathcal{T}_{34} \\ \mathcal{T}_{41} & \mathcal{T}_{42} & \mathcal{T}_{43} & \mathcal{T}_{44} \end{pmatrix} \begin{pmatrix} p^1 \\ p^2 \\ q^1 \\ q^2 \end{pmatrix} = \begin{pmatrix} a^1 \\ a^2 \\ b^1 \\ b^2 \end{pmatrix}, \tag{10}$$

where the elements of $\mathcal{T}$ describe the coupling between different multipolar components. For more scatterers or when considering a higher number of multipole moments for each meta-atom, the matrix needs to be extended, respectively. Note that the $\mathcal{T}$-matrix formulation in Eq. (10) can be linked to the T matrix in Eq. (3) via the addition theorem for vector spherical harmonics [49], which can be written as

$$T = W\mathcal{T}W^{L}, \tag{11}$$

where W denotes the translation operator from local coordinate 1 and 2 to the global coordinates, which has been used as a referential coordinate system in Eq. (3). The matrix on the right side, W^L denotes the left inverse of W. The left inverse is also called Moore-Penrose pseudoinverse, defined as $W^L = (W^\dagger W)^{-1}W^\dagger$, where $W^\dagger$ is the transpose conjugate of W.

C. Eigenvalue formulation

To study the optical properties of meta-atoms detached from a specific illumination as well as the coupling between meta-atoms, we use on the one hand the basis set obtained from diagonalizing the local $\mathcal{T}$ matrix

$$\mathcal{T} = XHX^{-1}. \tag{12}$$

Here X is a matrix whose columns are eigenvectors of $\mathcal{T}$. H is a diagonal matrix whose diagonal components are the eigenvalues of the matrix $\mathcal{T}$. Note that an identical expression holds when considering the global T matrix.

In both possible eigenvalue problems, the square of the absolute eigenvalue $|\eta_i|^2$ divided by ω^2 is proportional to the strength of a particular mode sustained by the meta-atom or the coupled system, respectively. This eigenvalue is the primary quantity of interest. The eigenvalues in global and local coordinates can be linked by (the proof is given in Appendix A)

$$H^{\mathrm{glo}} = Z^{-1}WH^{\mathrm{loc}}W^{L}Z, \tag{13}$$

where Z are the eigenvectors of $(WH^{\mathrm{loc}}W^{L})$ and H^{glo} and H^{loc} are diagonal matrices containing the eigenvalues

in global and local coordinates, respectively. The matrix $Z^{-1}W$ and $W^{L}Z$ can be understood as projection matrices that transform the modal strength of a particular mode (its eigenvalue) from local coordinates to global coordinates. It is important to note that these matrices are, in general, rectangular matrices. This means that for a given number of expansion orders, the local coordinates always (except if there is only single particle) contain more modes when compared to the global coordinates. The modes in global coordinates, therefore, can be understood as the sum of the projection of the modes in local coordinates. Note that the exact locations of each particle are needed to transform the eigenvalue from local to global coordinates and vice versa.

For the T matrix, i.e., in a global coordinate system, the far field scattering contribution of that mode is proportional to this eigenvalue. The actual scattering cross section σ_{sca} for a given incident field expanded into vector spherical harmonics can be decomposed into the eigenvectors of the T matrix via

$$\sigma_{\text{sca}} = \frac{4\pi}{k_b^2} \sum_i \sum_j \eta_i \eta_j^* \langle G|X_j\rangle \langle X_i|G\rangle \langle Y_i|Y_j\rangle , \tag{14}$$

where G denotes the coefficients of the incident field $\binom{p}{q} = G$, Y_i denotes the eigenvector of the transpose conjugate of the T matrix, and $\langle X_i|X_j\rangle$ denotes the inner product of vector X_i and X_j. Such formulation is necessary to accommodate the non-Hermitian character of the T matrix [43]. On the other hand, in the local coordinates description, the scattering cross section can be decomposed as (proof will be given in Appendix B)

$$\sigma_{\text{sca}} = \frac{4\pi}{k_b^2} \sum_f \sum_g \eta_g \eta_f^* \langle G|X_f\rangle \langle X_g|G\rangle \langle Y_f|W^\dagger W|Y_g\rangle , \tag{15}$$

where, in contrast with the expression in Eq. (14), each variable corresponds to the variable obtained in the local coordinate (i.e., η is now the eigenvalue of T matrix). For the same expansion order, the summations are J times larger than the summation required for the decomposition using modes obtained from a global coordinates description. Note that the cross coupling related weight ($\langle Y_f|W^\dagger W|Y_g\rangle$) now also depends on the translation operator (W) from local to global coordinates. From Eq. (15), the eigenvalue can also be interpreted as how easy the modes can be excited from outside (modal strength). The second part of the equation in the right-hand side ($\langle G|X_f\rangle \langle X_g|G\rangle$) tells us the information of how the incident field couples to the modes. Finally, the last part ($\langle Y_f|W^\dagger W|Y_g\rangle$) denotes how the modes coupling to each other and more importantly, as opposed to the expression in Eq. (14), for the same mode, the value of $\langle Y_i|W^\dagger W|Y_i\rangle$ in general will not be one, as it depends on the translation operator W. This suggests the importance of the location of each particle when considering its impact in measurable quantities, such as scattering cross section.

Each eigenvector X_i contains information on the multipolar composition of the particular mode. This holds for both the local and the global formulation. Since the decomposition of the T matrix is done independently with respect to the frequency, a mode tracking algorithm needs to be used that links the eigenmodes found at each frequency. In our work, we track the modes by calculating at first all eigenvalues for a small number of n frequencies $(f_1, f_2, \ldots, f_{n-1}, f_n)$. Typically a value of $n = 5$ is used. The eigenvalues are then assigned to belong to a specific mode upon visual inspection. Far away from any resonance frequency of the system, the proper assignment does not constitute a problem, as the eigenvalue of the eigenmodes are well separated in amplitude. Then, an automatic procedure is applied to track the modes for increasing frequencies. For this purpose, the amplitudes of the modes at n lower frequencies are fitted with a polynomial of order $n-2$. The corresponding mode for frequency f_{n+1} is the mode with an eigenvalue that is closest to the extrapolated eigenvalue of all modes obtained from such fitting. This allows us to link the newly calculated eigenvalues in an automatic manner to the eigenvalues of the same mode calculated at lower frequencies. For degenerate eigenvalues, a refined mode tracking algorithm is used, where the inner product of the corresponding degenerate modes for frequency f_n and f_{n+1} are used. Here the maximum value of inner product between eigenvector of mode i for frequency f_n and all eigenvectors for frequency f_{n+1} denotes the mode i for frequency f_{n+1}.

III. STUDY OF SELECTED META-ATOMS

After introducing the methodology, we will apply it now to selected hierarchical self-assembled meta-atoms. Throughout this paper, we consider gold nanospheres embedded in air. The permittivity of gold is considered by means of a Drude model as

$$\varepsilon_{\text{Au}} = \varepsilon_\infty - \frac{\omega_p^2}{\omega(\omega + i\gamma)}. \tag{16}$$

Here $\varepsilon_\infty = 9$, $\hbar\omega_p = 9$ eV, and $\hbar\gamma = 0.05$ eV [50]. We stress that we use a spectral method and, in general, at each frequency a permittivity can be considered that is independent from the permittivity at other frequencies. Using a Drude model is done here rather for convenience. It provides a smooth dependency of all quantities of interest on the frequency and is not affected by experimental details of the permittivity function.

In the following, we start with the trivial example of an isolated sphere. We continue by considering two coupled spheres to highlight the features that can be observed in the hybridization of the modes. Then, we study a single hierarchical meta-atom and finally the hybridization of two coupled hierarchical meta-atoms. We consider as an example for a hierarchical meta-atom a core-shell particle where a shell made from metallic nanoparticles decorates a core sphere. The structure is canonical in a sense that it allows us to induce a strong magnetic dipole moment. It has been investigated both theoretically and experimentally [27,51,52].

A. Sphere

For a single sphere there exists an analytical solution for the scattering strength of a particular mode. This is given through the Mie coefficients. Each mode is composed out of a single vector spherical harmonic. No cross coupling occurs because of the high symmetry of the problem. Therefore, the T matrix is already diagonal.

The modal strength and the projection parameter $c_i = 4\pi c^2 |\langle G|X_i\rangle|^2$, which describes how an incident field couples to mode i, are shown in Figs. 1(a) and 1(b), respectively. Note that, since for a single sphere the T matrix is a diagonal matrix, the cross coupling terms in Eq. (14) ($\langle Y_i|Y_j\rangle$ for $i \neq j$) are zero. It suggests that the mode scattering strength only depends on the projection of the incident wave and the eigenvalue of the related eigenvector. It can be seen that the system is dominated by both electric multipolar [dipole (D_e) and quadrupole (Q_e)] components and also to a smaller extent by a magnetic dipole mode (D_m). It can be seen that the scattering cross section can be linked directly to the strength of the modes. This in turn can be linked to the eigenvalues of the T matrix. Since we have a symmetric system, we expect the appearance of several degenerate modes. For example, modes consisting of a purely D_e^x have the same modal amplitudes as D_e^y modes, where the superscript denotes the direction of the dipole moment. From these values, it is also possible to study the related scattering cross section of the structure. The scattering cross section obtained from a modal decomposition $\sigma_{\text{sca}}^{\text{eig}}$, as well as the scattering cross section obtained directly from the T matrix using Eq. (3), $\sigma_{\text{sca}}^{\text{dir}}$ [by using the corresponding expansion coefficients of incident field in Eq. (3)] of a single sphere illuminated by a linearly polarized plane wave are shown in Fig. 1(c). It can be seen that the direct calculation from the T matrix and the modal decomposition yield the same result.

The magnitude difference between eigenvalue simply denotes how easy a mode can be excited. A bigger sphere will have a stronger response compared to a smaller sphere, and this fact is linked directly into the eigenvalue of the T matrix, as all the eigenvectors are normalized. This fact can be understood from Eq. (14), where the scattering cross section depends on the eigenvalue as well as on the projection of the incoming wave to the eigenvectors. As a larger sphere will scatter more light, its eigenvalue will be larger when compared to the eigenvalue of a smaller sphere.

B. Coupled spheres

We continue to apply both formulations of a local $\mathcal{T}$ matrix and a global T matrix to study a dimer made of gold nanospheres. The basic geometry is illustrated in the inset of Fig. 2. To simplify the problem, we calculate the modes for a dimer within dipole approximation (that is, $N = 1$). We model our dimer as two gold spheres with radius 3 nm and with a center-to-center distance of $d = 7$ nm. The sizes were purposely chosen to allow for a comparison to ordinary hybridization theory. But this is by no means a limitation. The transfer-matrix formulations of Eqs. (3) and (10) will be used and we will highlight the differences between the two approaches.

Figure 2(a) show the modal strength obtained with global formulation. Again, the quantity that is plotted corresponds to the square of the absolute eigenvalue $|\eta|^2$ divided by ω^2. Three peaks are observed. Two of these peaks are distinct in that they have a much stronger magnitude. The third one can only be seen on a logarithmic scale. The stronger peaks correspond to modes with a dominant electric dipole contribution. This explains why their magnitude is so much stronger, since for sufficiently small particles, only the electric dipole will survive. Therefore, the excitation of such modes

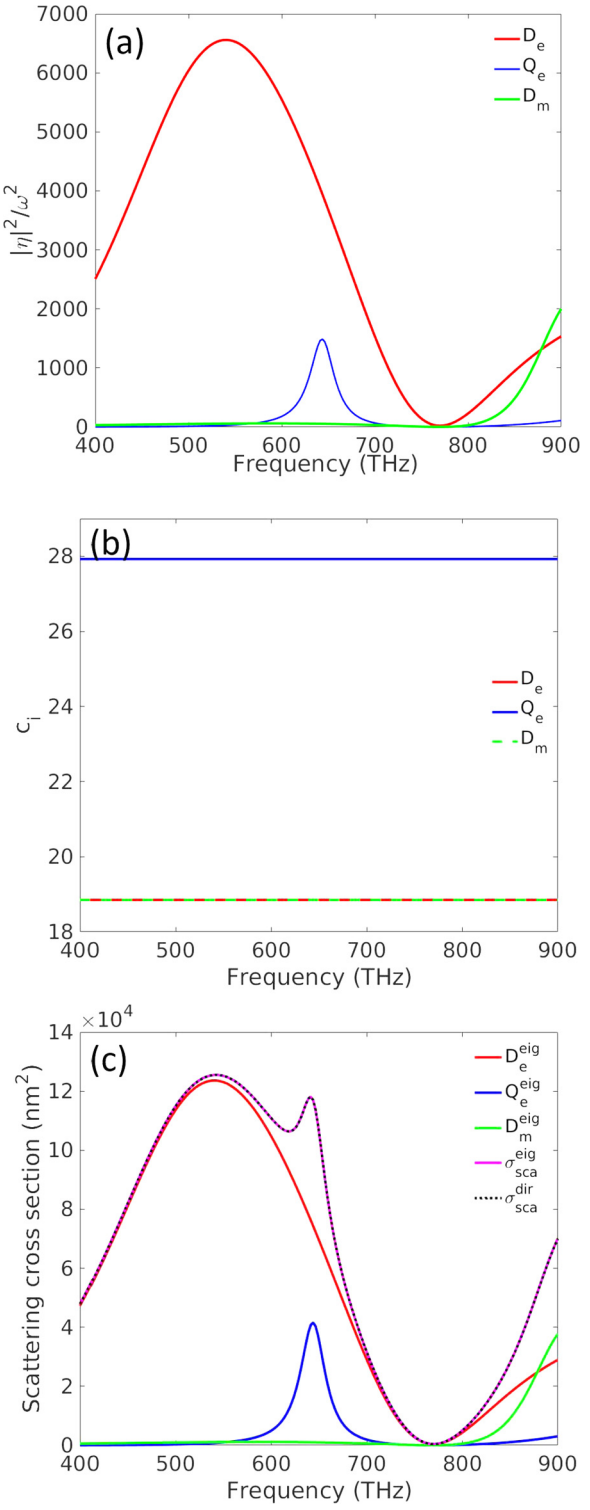

FIG. 1. (a) Modal strength for each eigenmode of a small gold sphere with a radius of $R = 90$ nm. D_e, D_m, and Q_e denote electric dipole, magnetic dipole, and electric quadrupole contributions, respectively. (b) The projection parameter of the incident plane wave onto the eigenvector of each mode and (c) modal decomposition of the scattering cross section. Results from the modal decomposition are compared to the direct solution. Perfect agreement is found.

is most likely. The individual dipoles of the spheres are in phase with each other. One parallel to the connecting axis and

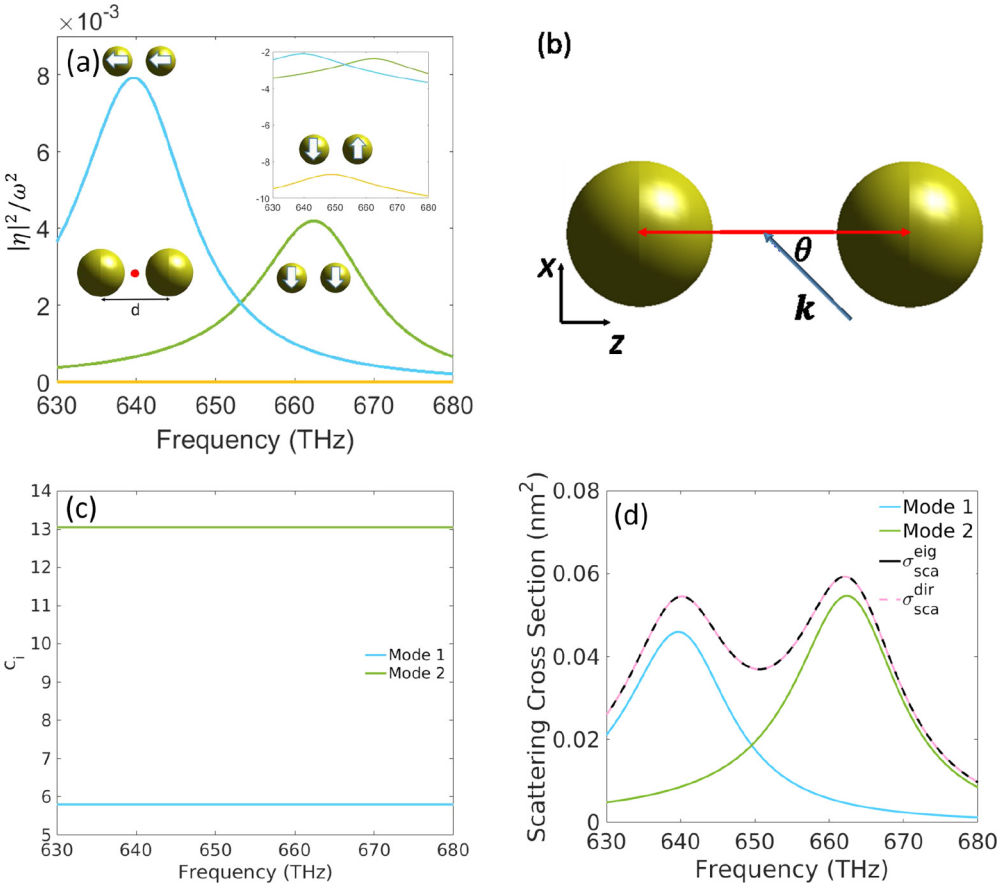

FIG. 2. (a). Modal strength obtained using T matrix in the global coordinate system [Eq. (3)]. The red dot denotes the coordinate system used to calculate the transfer matrix. Different modes are characterized by different colors. The inset in (a) shows the same quantity but in a logarithmic scale. (b) The scattering scenario of dimer structure, where the incident field is a plane wave with wave vector denoted by the red arrow with $\tan\theta = \frac{2}{3}$ and the electric field of the incident field always in x-z plane. (c) Projection parameter of the incident field described in (b) onto eigenmodes of the structure and (d) the decomposition of scattering cross section to each eigenmode of the structure in global coordinate [Eq. (14)]. Comparison to a direct solution is equally obtained and excellent agreement is found.

another one perpendicular to it. The third mode is dominated by a magnetic dipole contribution in the central coordinate. It has a much weaker magnitude. For that mode, the individual electric dipole moments of the spheres are perpendicular to the connecting axis and point in opposite direction, i.e., they are π out of phase.

To link the modal strength to observable quantity, we take as an example the scattering response from dimer structure as described in Fig. 2(b). Here the amplitude of the incoming field is normalized and the wave vector makes an angle θ to dimer axis, as described in the caption. Using this scenario, the projection parameter as well as the modal decomposition of the scattering cross section for a certain illumination scenario are shown in Figs. 2(c) and 2(d), respectively. Here mode 1 (2) denotes the mode with resonance at 639.6 (662.5) THz. As the contribution from the mode with resonance frequency around 648 THz is negligible, we omit this mode contribution in the figure. In the case of the dimer structure, the global coordinate modes are still orthogonal to each other, which implies that the coupling terms in Eq. (14) are zero. This makes the analysis much easier. We see that the scattering cross section of the dimer in this illumination scenario is mainly due to the contribution from two modes. These modes denote the modes that are in phase with each other, which results in a stronger modal strength compared to the other mode.

By diagonalizing the $\mathcal{T}$ matrix in Eq. (10), it is possible to capture further modes supported by the dimer, as seen in Fig. 3(a). There we obtain four distinct resonances which correspond to the modes with different dipole orientation. Three of these modes correspond to the modes as seen in the global formulation. The resonance frequencies match exactly. The fourth mode, which is not seen in the global formulation, is a mode where the two dipole moments are out of phase and they are parallel to the connecting axis. Such in-plane orientation will lead to an electric quadrupolar response that is not captured when formulating the global T matrix in dipole approximation. It occurs, of course, once the quadrupole terms are taken into account as well.

The amplitude differences in the eigenvalues shown in Figs. 2(a) and 3(a) are the result of the coordinate transformation from the local coordinate of each subsystem to the global coordinate, as described in Eq. (13). Physically, it can be understood as how the effective modal strength (in the global coordinate) can be decomposed into excitations from its individual subsystem, i.e., it measures the modal strength

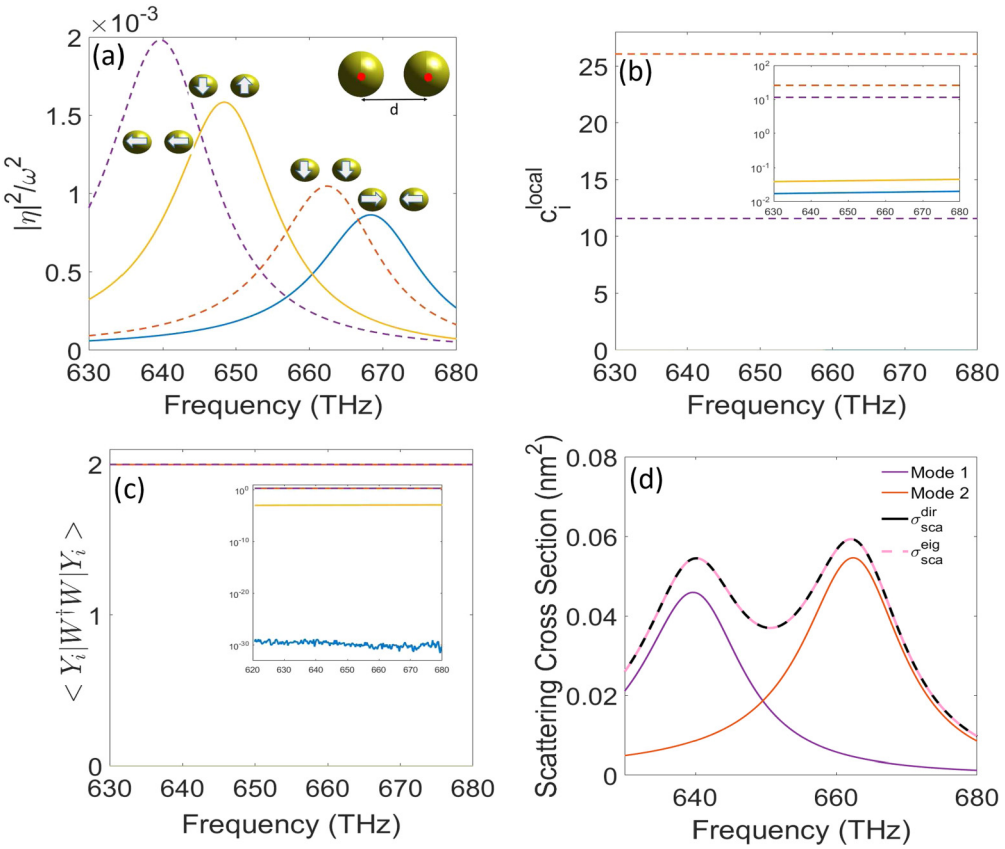

FIG. 3. (a). Modal strength obtained using $\mathcal{T}$ matrix in the local coordinate system [Eq. (10)]. The red dot denotes the coordinate system used to calculate the transfer matrix. Different modes are characterized by different colors. (b) Projection parameter of the incoming field described in Fig. 2 onto eigenmodes of local $\mathcal{T}$ matrix, (c) the self-coupling terms $\langle Y_i|W^\dagger W|Y_i\rangle$ for each eigenmode obtained from $\mathcal{T}$ matrix, and (d) the decomposition of scattering cross section to each eigenmode of the structure in local coordinate [Eq. (15)]. Comparison to a direct solution is equally obtained and excellent agreement is found.

of the entire ensemble. In contrast, the modal strength in the local coordinate expresses how easy a mode in each of the subsystems can be excited. The same mode can exhibit different properties depending on the projection operators that linked the local and global coordinate formulation. For example, let us consider the modes where both electric dipole moments sustained in the individual spheres are in phase with each other (639.6 and 662.5 THz). In the local coordinate, the amplitude of the modal strengths ($|\eta|/\omega$) are around $\sqrt{2}$ and 1, respectively. Since in both cases, the electric dipoles are in phase and we have two identical subsystems, intuitively, the total modal strength in the global coordinate of these modes has to be the sum of both of them. This gives us the value around $2\sqrt{2}$ and 2, or in terms of ($|\eta|^2/\omega^2$), 8 and 4, exactly as observed in Fig. 2(a). In contrast, the opposite is observed for the mode sustained at the frequency of 648.3 THz. For this mode, the electric dipoles oscillate π out of phase. The net electric dipole moment of this mode in the global coordinate system is zero. But this configuration is characterized by a notable magnetic dipole moment in the global coordinate. But as the magnetic dipole moment can only be weakly excited because the particle is so small, it explains why the amplitude of such mode in the global coordinate system has several orders of magnitude difference compared to the same mode in the local coordinate system.

On the other hand, it is also possible to decompose the scattering cross section into modes obtained from a local coordinate description, as can be seen in Fig. 3. In this case, the modes with resonance frequency around 648 and 670 THz are particularly interesting. Even though their modal strengths (η) are comparable to the other two modes, the projection of scattering cross section to both modes are negligible. This happens because of two factors. The projection of incident field c_i^{loc} onto eigenmodes of the structure [as seen in Fig. 3(b)] and the self-coupling term $\langle Y_i|W^\dagger W|Y_i\rangle$ [Fig. 3(c)] are very small for both modes. As the scattering cross section is the result of a multiplication of all the factors contained in Eq. (15), the contribution of both modes can be neglected. It is shown here that, by analyzing the modal strength and projection parameter, it is possible to engineer the response of the structure (for example, to excite just a single mode in the structure). Finally, it can be concluded that the final observable quantity will always be the same, irrespective of the chosen local or global formulation. Of course, this requires a sufficient large number of orders to be retained in the expansion.

For a given maximum multipolar order, the matrix size of the local approach is larger than for the global approach. This explains why more modes can be identified in the local approach. Increasing the multipolar order of the global approach would recover the missing modes.

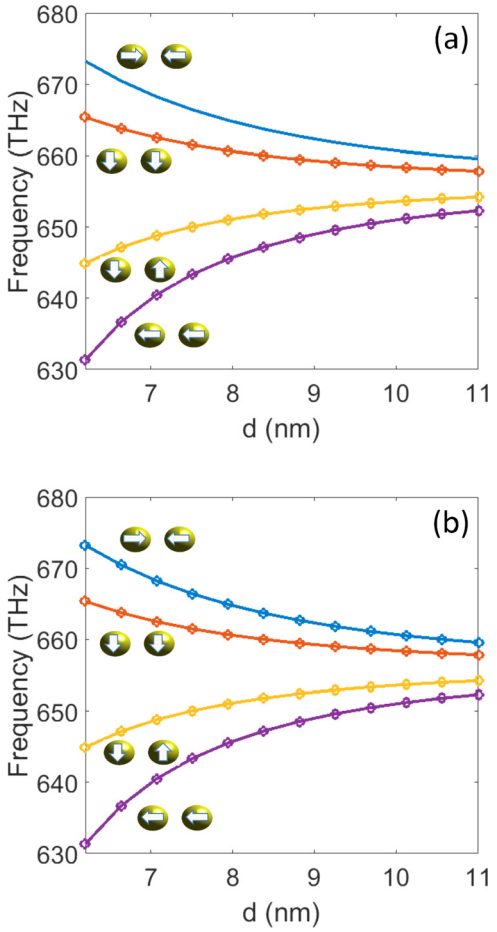

FIG. 4. Peak position (circles) of the different modes as obtained from the diagonalization of the T matrix in (a) global or (b) local formulation and the resonance position as predicted by hybridization theory (straight line) for the dimer structure.

The validity of both formulations (T or $\mathcal{T}$) can be assessed by varying the distance between the spheres, extracting the spectral resonance frequencies of the respective modes, and by comparing it to the resonance position obtained using hybridization theory [50] (as shown in Fig. 4). The functional dependency of the spectral position of the modes perfectly agrees among the different methods. In Fig. 4 it can be seen that when using a global coordinate system and while sticking to dipole approximation, we miss the fourth mode, as this mode effectively is a quadrupole mode with respect to a central coordinate, as discussed before. This problem does not occur if we employ the local formulation as this method captures the response of each individual sphere.

Using our method based on the diagonalization of the transfer matrix, it is possible to study the hybridization of particles with an arbitrary size beyond the quasistatic approximation. This is shown in the following section, where the modes of a hierarchical meta-atom and its coupling to a second meta-atom are discussed.

C. Cluster of spheres

The considered self-assembled meta-atom consists of 60 gold nanospheres. A conceptual sketch is shown in Fig. 5. Each nanosphere has a radius of 20 nm. The nanospheres

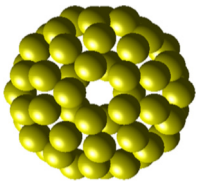

FIG. 5. Geometry of the considered self-assembled meta-atom. It is made of a larger number of nanoparticles that reside on top of a spherical surface.

are assembled on top of a virtual sphere with a radius of 76 nm. These nanospheres are ordered in a highly symmetric way, as defined in Ref. [32]. Such a symmetric assembly of nanoparticles preserves the degeneracy of the modes, which assists their understanding. The analysis of the modes of the isolated meta-atom is done by using the formulation of a global T matrix with respect to the center of the cluster. Previously, the study of clusters of spheres using their T matrix has been done by calculating the scattering response of such a structure [53]. In this paper, however, we take a different approach by identifying the mode of the structure via their T matrix, as will be discussed in the following paragraphs.

Since the size of the corresponding meta-atom is comparable to the wavelength of interest, the meta-atom cannot be described by quasistatic approximation anymore. Here we show the versatility of this approach by calculating the T matrix while retaining modes up to the fourth multipolar order. Figure 6 shows the modal strength of the dominant modes (eigenvalues divided by ω^2) calculated using dipole approximation ($N = 1$) as well as the strength of the three dominant modes using a higher order correction ($N = 4$). D_e and D_m are electric and magnetic dipole modes, respectively. For $N = 1$ the modes obviously have a dipolar character only. By increasing the multipolar order, the modes tend to have contributions from different vector spherical harmonics.

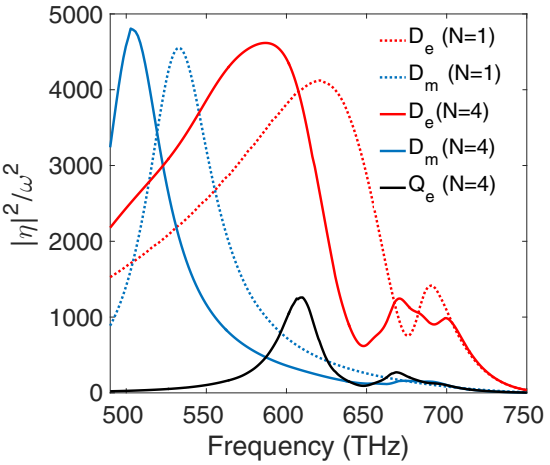

FIG. 6. Frequency dependent strength of the three dominant modes that were found from diagonalizing the global T matrix of the meta-atom. We distinguish a mode that is dominated by an electric dipole contribution (red line), a mode that is dominated by a magnetic dipole contribution (blue line), and a mode that is dominated by an electric quadrupole contribution (black line).

However, the contribution from dipole terms are still dominant to these modes, i.e., larger than 80%. Therefore, we still call them the electric and magnetic dipolar modes. Moreover, the spectral position of their resonances changes slightly and additional peaks appear in their spectrum. These are small modifications that occur due to the finite size of the meta-atom. An electric quadrupole mode (Q_e) also appears. We emphasize that each dipolar mode is threefold degenerate due to the highly symmetric arrangement.

To understand the resonance structure in more detail, we fit the spectral dependency of the dipolar modes to the coherent sum of multiple Lorentzian oscillators. Each of these oscillators shall correspond to a specific type of resonance sustained by the meta-atom in the specific dipolar scattering channel. For this purpose, we fit in a least-square sense the strength of the modes to the following functional dependency:

$$f(\omega) = \omega^2 \left| \sum_{n=1}^{L} \frac{f_n}{\omega_n^2 - \omega^2 - i\gamma_n \omega} \right|^2. \tag{17}$$

Here the nth Lorentz oscillator is characterized by its oscillator amplitude f_n, a central frequency ω_n, and a damping coefficient γ_n. Note that the multiplication factor of ω^2 appears as a direct consequence of the scaling of the eigenvalue of the T matrix.

The magnetic dipole mode, shown in Fig. 6, can be reproduced by a single Lorentzian oscillator, i.e., if plotted above each other the curves are indistinguishable. The resonance frequency of that mode is 500.9 THz.

The spectral position and the emergence of such resonance can be understood if we consider the shell made out of the nanospheres as an effective medium. Its effective permittivity can be expressed using Clausius-Mossoti effective medium theory. It expresses the effective permittivity of an ensemble of spheres as

$$\varepsilon_{\text{eff}}(\omega) = \varepsilon_{\text{b}} \frac{3 + \frac{2N\alpha(\omega)}{V}}{3 - \frac{N\alpha(\omega)}{V}}, \tag{18}$$

where $\varepsilon_{\text{eff}}(\omega)$ is the effective permittivity, ε_{b} is the background permittivity, $\alpha(\omega)$ is the electric polarizability of a single nanosphere, and $\frac{N}{V}$ is the filling fraction, i.e., the number of nanoparticles N per volume V.

The effective permittivity of the pertinent shell material is shown in Fig. 7. We observe a Lorentzian resonance around a central frequency of 592 THz, given by the resonance frequency of the localized surface plasmon polariton sustained in each nanoparticle. At smaller frequencies, the permittivity is large and positive. For a magnetic mode resonance to occur, the only option is to excite a magnetic Mie-type resonance in the object that consists of a shell with a given thickness made from the effective medium just discussed. The Mie resonance occurs at frequencies with a large and positive permittivity. This is just what we observe in Fig. 6.

The story is not that easy for the electric dipole mode. Indeed, at first glimpse three resonances seem to appear. A strong resonance occurs and two weaker ones are coherently modulated on top of it at higher frequency. By performing a fit with three Lorentzians, we encountered insufficient agreement with the actual strength of the electric dipole mode. A much better agreement was found when using five Lorentzian oscillators. The magnitude of the electric mode along with the five individual Lorentzians used to fit the response is shown in Fig. 8.

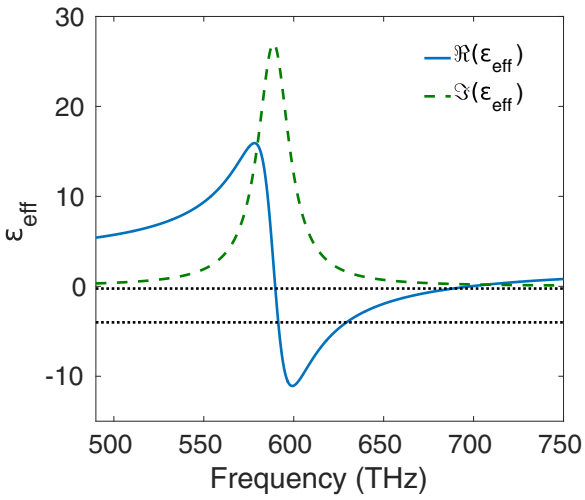

FIG. 7. Effective permittivity of a medium made of gold nanospheres with a radius of 20 nm embedded in air. The filling fraction was obtained by equating the total volume of the nanospheres and the volume of the spherical shell (with inner radius 76 nm and outer radius 116 nm). The black dotted lines represent the plasmonic resonance conditions of the layered sphere in dipole approximation using resonance conditions derived in [54].

Similarly as before, the five Lorentzians can be explained when considering the resonances as sustained by a shell made from a material with a dispersive permittivity as shown in Fig. 7. First of all, in this figure we have marked with dashed lines those permittivity values that would allow us to observe a plasmonic resonance in a metallic shell with the considered geometry. These permittivities can be derived from a quasistatic analysis [54]. In principle, the dispersion of the shell material attains these values at four different frequencies.

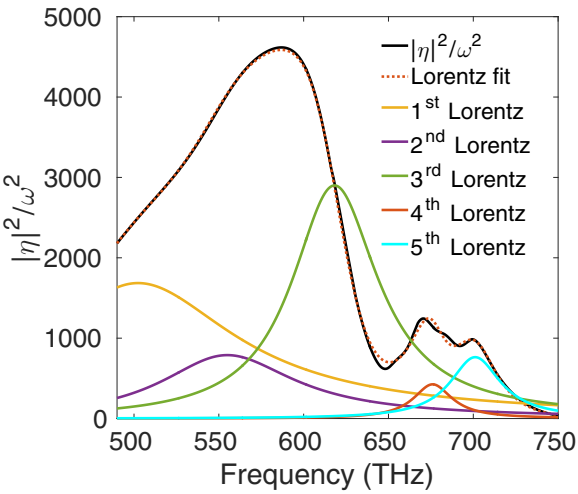

FIG. 8. Magnitude of the electric dipole mode as obtained from the eigenvalue analysis of the T matrix and its decomposition into five Lorentzian oscillators.

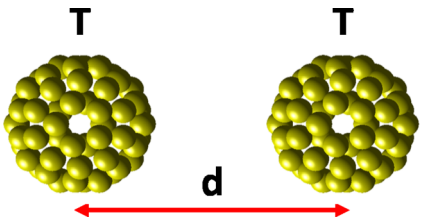

FIG. 9. Geometrical details of the two clusters of spheres that are considered.

From the five Lorentzians, the third (@ 618.4 THz) and the fifth (@ 701.1 THz) match closely to the two possible frequencies where the necessary dispersion is offered by the shell material. These frequencies are far away from the actual resonance frequency of the shell material where absorption is quite weak. Hence, the resonance are well resolved. The two further frequencies predicted here are close to the resonance where absorption is high. This prevents the notable excitation of a plasmonic mode at these frequencies.

Besides these two Lorentzians with electric dipolar plasmonic origins, we notice that two further Lorenzians have resonance frequencies in the spectral region where the permittivity of the shell material attains positive values. This suggests that the first Lorentzian (@ 502.6 THz) and the second Lorentzian (@ 555.3 THz) correspond to electric type Mie resonance that require for their excitation a large and positive permittivity.

The last remaining Lorentzian mode, i.e., the Lorentzian mode that is expressed by the fourth Lorentzian (@ 676.6 THz), is a dominantly electric quadrupolar plasmonic mode that also has a small electric dipolar contribution. Overall this Lorentzian mode is weakly excited but it needs to be considered.

D. Coupled cluster of spheres

In this section we study the coupling between two self-assembled meta-atoms. Figure 9 shows a sketch of the considered geometry. We vary the distance between the clusters and calculate the modes of the system by employing first, Eq. (3) for each individual meta-atom with respect to its central coordinate and second, this T matrix as an input to construct the $\mathcal{T}$ matrix. It expresses the $\mathcal{T}$ matrix of the entire system in a local formulation. Modal strength of this $\mathcal{T}$ matrix are presented. To simplify the discussion, we only focused on the "effective" dipole response of each meta-atom, as the hybridization between them can be already clearly observed, as depicted in Fig. 10.

The modal strength of the modes formed due to the coupling between two clusters of spheres is shown in Fig. 11 for a selected distance. Here we see that the degenerate modes observed for a single cluster of spheres split into new modes formed due to the coupling between the clusters, as observed also in the dimer structure. The response is overall is quite complex and further insights are only possible when decomposing the response again into Lorentzian resonances.

Figure 12(a) shows the resonance positions of the Lorentzian decomposition of the electric dipole modes that occur upon hybridization [ω_n as described in Eq. (17)]. We only focus on the three most dominant Lorentzian contributions of the modes that occur at lower frequencies. Figure 12(b) shows the resonance positions of the magnetic dipole modes that occur upon hybridization. The resonance positions were extracted from Lorentzian fits of the respective modal strength of the mode that was obtained from diagonalizing the $\mathcal{T}$ matrix, i.e., the kind of data that was shown in Fig. 11 for a selected separation between the clusters. For each mode of the isolated meta-atom, it will split into four modes, which always correspond to an in phase and out of phase excitation of the dipole moment in each individual cluster, as depicted in Fig. 10. The dipoles can be arranged parallel or perpendicular to the connecting axis, giving rise to the complicated spectra, i.e., they are in phase or out of phase. The spectral positions of these modes sensitively depend on the distance between the two meta-atoms. Oscillation of these mode frequencies can be seen when the meta-atoms approach each other. They can be associated with the constructive and destructive interference between the reflected waves from one meta-atom to another.

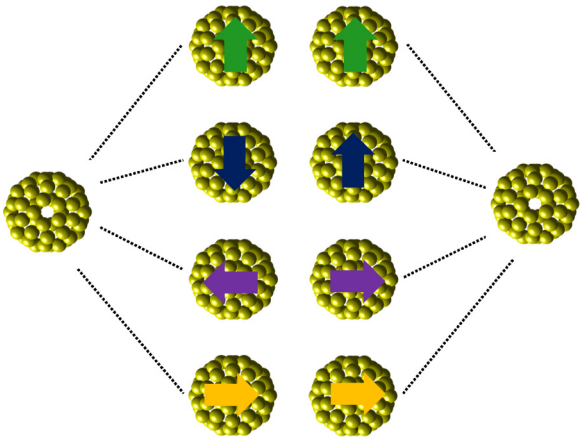

FIG. 10. All possible modes for hybridization of electric or magnetic dipole of the two cluster system.

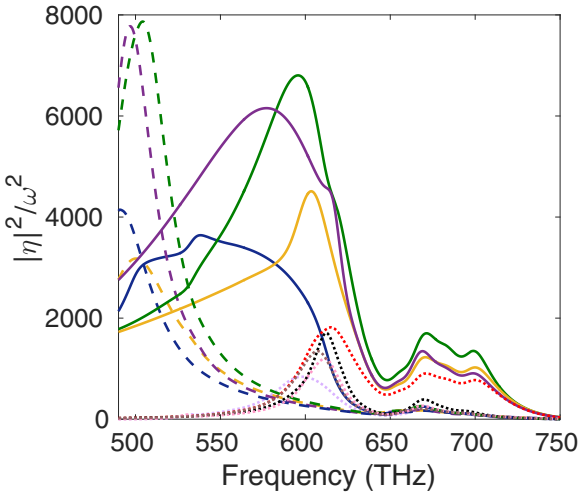

FIG. 11. Modal strength of each hybridized mode of two clusters of spheres with $d = 301$ nm. The dashed (solid) lines correspond to magnetic (electric) dipole modal strength, while the dotted lines show the hybridized mode of electric quadrupole.

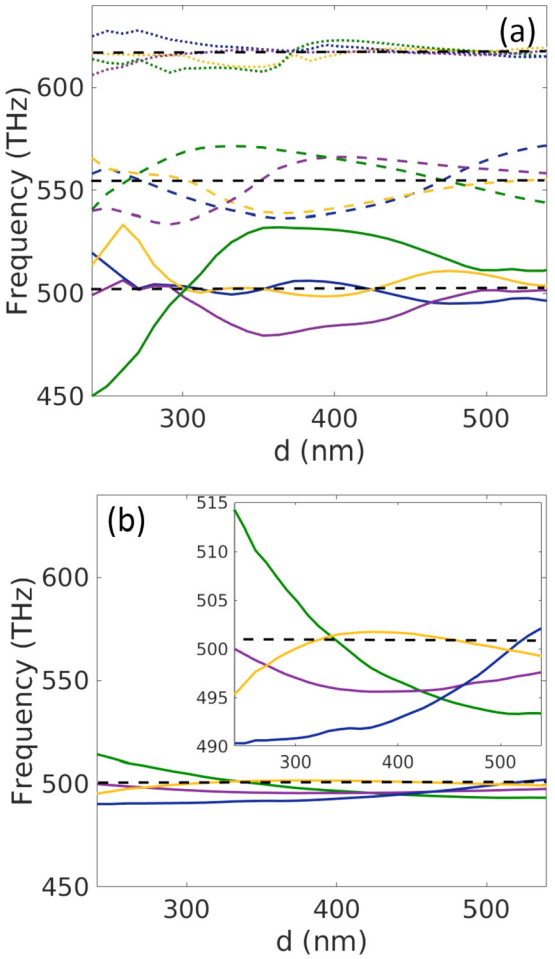

FIG. 12. Peak positions of (a) three dominant Lorentzians from the decomposition of the hybridized electric dipole modes and (b) hybridization of magnetic dipole modes. The colors correspond to the modes as shown in Fig. 10. The black lines correspond to the resonance frequencies of the isolated meta-atom.

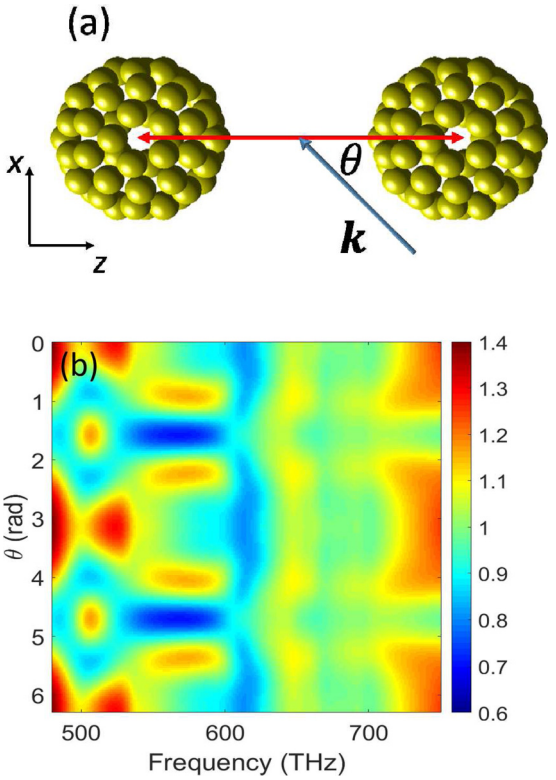

FIG. 13. (a) Schematic view of a scattering scenario of two clusters of spheres where the distance between the clusters is 301 nm (the electric field of the incident field always in x-z plane) and (b) the scattering enhancement for a different illumination scenario.

It is important to note that the electric dipole interactions have a much stronger impact compared to magnetic ones. This can be seen from the oscillation of the resonances in the coupled meta-atoms with respect to the resonances of the isolated meta-atom. Whereas the resonance frequency of the dominant electric modes shift by up to 90 THz, the magnetic modes shift only by up to 25 THz. The resonance frequencies of the magnetic modes of the hybridized systems are less dispersive and less sensitive to the coupling with a nearest neighbor.

A similar behavior has been observed in Ref. [55] and theoretically explained in Ref. [56] for planar metasurfaces. There, the introduction of spatial disorder into a system of periodically arranged meta-atoms that have both an electric and magnetic resonance had a much weaker impact on the magnetic response when compared to the electric response. The magnetic resonance indeed was quite insensitive against disorder in the system. The reason for the weaker response has been the dominant contribution of nonradiative losses to the magnetic resonance. When compared to the total losses, less scattered field is generated at the magnetic resonance when compared to the electric resonance. The effective dispersion in the magnetic permeability of the metasurface has been largely independent on the degree of disorder. This suggests that these meta-atoms, when operated at their magnetic resonance frequency, virtually do not see their nearest neighbors. Since we observe a similar behavior in the coupling process among self-assembled meta-atoms, we can expect that the effective properties of a metamaterial made from these meta-atoms does not degrade upon tight packaging. Large filling fractions can be realized without causing a degradation. Coupling to nearest neighbors does not deteriorate to a notable extent the magnetic dipolar resonance properties when compared to the isolated meta-atom. This is an important finding towards the realization of densely packed self-assembled meta-atoms.

The scattering response of the two coupled meta-atoms can be compared to the scattering response of two individual meta-atoms. In this context, it is easier to discuss the scattering enhancement factor β defined here as

$$\beta = \frac{\sigma^{cc}}{2\sigma^{i}}, \tag{19}$$

where σ^{cc} denotes the scattering cross section of the two clusters and σ^{i} is the scattering cross section of an individual cluster. The dependency of β on the frequency and for various incident field scenarios, as depicted in Fig. 13(a), can be seen in Fig. 13(b). Here, due to the symmetry breaking of the system, the scattering response depends on the incoming angle θ. Depending on θ and frequency, the scattering can be

reduced or enhanced with respect to the scattering from the two isolated subsystems. This makes it a perfect platform for applications which require the tunable properties of scattering response, e.g., to direct the emission of light with antennas to route information. We emphasise the fact that this analysis is quite conveniently done with the formalism we have developed here. The eigenmode analysis of the T matrix only needs to be done once; and the actual observable feature is calculated by projecting the incident field on the eigenmodes. This is an analysis that can be quickly done.

IV. CONCLUSIONS

We show that the diagonalization of the transfer matrix is a convenient tool to study the modes of isolated and coupled meta-atoms. The transfer matrix can be formulated in either a global or a local coordinate system. Both approaches are equally valid but are more insightful depending on a specific situation. The validity of this method has been checked by comparing spectral positions of plasmonic resonances to predictions made with hybridization theory. Emphasis was put in our work on studying the coupling between hierarchical meta-atoms as employed in the context of self-assembled metamaterials. It was shown that the dispersion of the individual modes occurs because of different resonances that are sustained in the meta-atom. Each of these resonances can be explained on physical grounds, which explains and quantifies the observed spectral features. Moreover, when studying the hybridization among modes in coupled self-assembled meta-atoms, it was found that the mode with a dominating magnetic dipolar contribution in the individual meta-atom is less sensitive against an interaction to a nearest neighbor. This is an encouraging finding to fabricate metamaterials out of these meta-atoms even at very high filling fractions. We stress the fact that the methodology is not limited in its application to a specific meta-atom. With that, the present work will provide impetus for the broader field of optical nanoantennas and plasmonics.

ACKNOWLEDGMENTS

This work was supported by German Science Foundation (Deutsche Forschungsgemeinschaft), Project No. RO 3640/4-1. R.N.S.S and M.F. also acknowledge support from the Karlsruhe School of Optics & Photonics (KSOP).

APPENDIX A: RELATION BETWEEN EIGENVALUE IN LOCAL AND GLOBAL COORDINATES

The eigenvalue decomposition of the $\mathcal{T}$ matrix can be written as

$$\mathcal{T} = X_{\rm loc} H^{\rm loc} X_{\rm loc}^{-1}. \tag{A1}$$

By arranging the term, left multiply both sides by the translation matrix W, and applying the fact that $W^L W = I$, the following equation can be obtained:

$$W\mathcal{T}W^L W X_{\rm loc} = W X_{\rm loc} H^{\rm loc}. \tag{A2}$$

The operator on the left-hand side $W\mathcal{T}W^L$ is just the T matrix in a global coordinate system. By proceeding further and applying the left inverse of the translation operator on both sides, and then proceed using the eigendecomposition of matrix $W H^{\rm loc} W^L = Z A Z^{-1}$, we arrived at

$$T W X_{\rm loc} W^L Z = W X_{\rm loc} W^L Z A. \tag{A3}$$

It can be seen that the eigenvalues in global coordinate $H^{\rm glo}$ is the diagonal matrix A. It can be concluded that

$$X_{\rm glo} = W X_{\rm loc} W^L Z, \tag{A4}$$

$$H^{\rm glo} = Z^{-1} W H^{\rm loc} W^L Z. \tag{A5}$$

From the above equations, it can be seen that the eigenvalues and eigenvectors in global coordinates depend on the transformation operator W. The matrix $Z^{-1}W$ and $W^L Z$ can be interpreted as transformation operators, which map the multipole moments from individual scatterers in local coordinates to the multipole moments of the entire structure in global coordinates. Note that, if W is an unitary matrix (which is the case for a single particle), the left inverse of W is just its inverse, $W^L = W^{-1}$. It can be proven easily that the matrix Z is the same as W (as matrix $W H^{\rm loc} W^L = W H^{\rm loc} W^{-1}$), which resulted in $H^{\rm loc} = H^{\rm glo}$ and $X_{\rm glo} = W X_{\rm loc}$. It can be proven in the same way that

$$X_{\rm loc} = W^L X_{\rm glo} W^{L^L} V, \tag{A6}$$

$$H^{\rm loc} = V^{-1} W^L H^{\rm glo} W^{L^L} V, \tag{A7}$$

where W^{L^L} is the left inverse of the left inverse of W and V is the eigenvectors of matrix $W^L H^{\rm glo} W^{L^L}$.

APPENDIX B: DECOMPOSITION OF SCATTERING CROSS SECTION IN LOCAL COORDINATE

The eigenvalue equation of the $\mathcal{T}$ matrix can be written as

$$\mathcal{T} \left|X_i\right\rangle = \eta_i \left|X_i\right\rangle. \tag{B1}$$

And for its transpose conjugate:

$$\mathcal{T}^\dagger \left|Y_i\right\rangle = \eta_i^* \left|Y_i\right\rangle. \tag{B2}$$

With the following bi-orthogonality relations hold:

$$\langle X_m | Y_n \rangle = \delta_{mn}, \tag{B3}$$

$$\sum_f \left|Y_f\right\rangle \langle X_f| = \sum_f \left|X_f\right\rangle \langle Y_f| = I. \tag{B4}$$

The scattering cross section is defined as

$$\sigma_{\rm sca} = \frac{4\pi}{k_b^2} \langle a|a\rangle = \langle T G^{\rm glo} | T G^{\rm glo}\rangle = \langle G^{\rm glo}|T^\dagger T|G^{\rm glo}\rangle. \tag{B5}$$

Applying the fact that $T = W\mathcal{T}W^L$, and using the fact that the incident field in local coordinate $|G_i^{\rm loc}\rangle = W^L |G_i^{\rm glo}\rangle$, we arrived at

$$\sigma_{\rm sca} = \frac{4\pi}{k_b^2} \langle G^{\rm loc}|\mathcal{T}^\dagger W^\dagger W \mathcal{T}|G^{\rm loc}\rangle. \tag{B6}$$

Now, applying the bi-orthogonality relation, the following equation can be obtained:

$$\sigma_{\text{sca}} = \frac{4\pi}{k_b^2} \sum_f \sum_g \langle G^{\text{loc}}|X_f\rangle \langle Y_f|\eta_f^* W^\dagger W \eta_g|Y_g\rangle \langle X_g|G^{\text{loc}}\rangle . \tag{B7}$$

By arranging term, we finally have

$$\sigma_{\text{sca}} = \frac{4\pi}{k_b^2} \sum_f \sum_g \eta_g \eta_f^* \langle G|X_f\rangle \langle X_g|G\rangle \langle Y_f|W^\dagger W|Y_g\rangle . \tag{B8}$$

[1] E. E. Narimanov and A. V. Kildishev, Appl. Phys. Lett. **95**, 041106 (2009).
[2] Z. Jacob, L. V. Alekseyev, and E. Narimanov, Opt. Express **14**, 8247 (2006).
[3] A. Alù, Phys. Rev. B **80**, 245115 (2009).
[4] P.-Y. Chen, J. Soric, and A. Alù, Adv. Mater. **24**, OP281 (2012).
[5] K. Hannam, D. A. Powell, I. V. Shadrivov, and Y. S. Kivshar, Phys. Rev. B **89**, 125105 (2014).
[6] V. Ponsinet, P. Barois, S. M. Gali, P. Richetti, J. B. Salmon, A. Vallecchi, M. Albani, A. Le Beulze, S. Gomez-Grana, E. Duguet, S. Mornet, and M. Treguer-Delapierre, Phys. Rev. B **92**, 220414 (2015).
[7] V. Yannopapas and I. E. Psarobas, J. Phys. Chem. C **116**, 15599 (2012).
[8] S. Tricarico, F. Bilotti, A. Alù, and L. Vegni, Phys. Rev. E **81**, 026602 (2010).
[9] Y. Liu and X. Zhang, Chem. Soc. Rev. **40**, 2494 (2011).
[10] R. A. Shelby, D. R. Smith, and S. Schultz, Science **292**, 77 (2001).
[11] V. M. Shalaev, W. Cai, U. K. Chettiar, H.-K. Yuan, A. K. Sarychev, V. P. Drachev, and A. V. Kildishev, Opt. Lett. **30**, 3356 (2005).
[12] S. Zhang, W. Fan, N. C. Panoiu, K. J. Malloy, R. M. Osgood, and S. R. J. Brueck, Phys. Rev. Lett. **95**, 137404 (2005).
[13] C. Enkrich, M. Wegener, S. Linden, S. Burger, L. Zschiedrich, F. Schmidt, J. F. Zhou, T. Koschny, and C. M. Soukoulis, Phys. Rev. Lett. **95**, 203901 (2005).
[14] P. A. Belov, R. Marqués, S. I. Maslovski, I. S. Nefedov, M. Silveirinha, C. R. Simovski, and S. A. Tretyakov, Phys. Rev. B **67**, 113103 (2003).
[15] S. S. Kruk, D. A. Powell, A. Minovich, D. N. Neshev, and Y. S. Kivshar, Opt. Express **20**, 15100 (2012).
[16] N. Liu, H. Guo, L. Fu, S. Kaiser, H. Schweizer, and H. Giessen, Nat. Mater. **7**, 31 (2008).
[17] Q. Wu and W. Park, Appl. Phy. Lett. **92**, 153114 (2008).
[18] J. A. Fan, C. Wu, K. Bao, J. Bao, R. Bardhan, N. J. Halas, V. N. Manoharan, P. Nordlander, G. Shvets, and F. Capasso, Science **328**, 1135 (2010).
[19] M. Gajc, H. B. Surma, A. Klos, K. Sadecka, K. Orlinski, A. E. Nikolaenko, K. Zdunek, and D. A. Pawlak, Adv. Funct. Mater. **23**, 3443 (2013).
[20] K. Sadecka, M. Gajc, K. Orlinski, H. B. Surma, A. Klos, I. Jozwik-Biala, K. Sobczak, P. Dluzewski, J. Toudert, and D. A. Pawlak, Adv. Opt. Mater. **3**, 381 (2015).
[21] L. De Sio, R. Caputo, U. Cataldi, and C. Umeton, J. Mater. Chem. **21**, 18967 (2011).
[22] L. De Sio, A. Cunningham, V. Verrina, C. M. Tone, R. Caputo, T. Bürgi, and C. Umeton, Nanoscale **4**, 7619 (2012).
[23] A. Kuzyk, R. Schreiber, Z. Fan, G. Pardatscher, E.-M. Roller, A. Högele, F. C. Simmel, A. O. Govorov, and T. Liedl, Nature (London) **483**, 311 (2012).
[24] S. Vignolini, N. A. Yufa, P. S. Cunha, S. Guldin, I. Rushkin, M. Stefik, K. Hur, U. Wiesner, J. J. Baumberg, and U. Steiner, Adv. Mater. **24**, OP23 (2012).
[25] K. Sadecka, J. Toudert, H. B. Surma, and D. A. Pawlak, Opt. Express **23**, 19098 (2015).
[26] J. Dintinger, S. Mühlig, C. Rockstuhl, and T. Scharf, Opt. Mater. Express **2**, 269 (2012).
[27] S. Mühlig, A. Cunningham, S. Scheeler, C. Pacholski, T. Bürgi, C. Rockstuhl, and F. Lederer, ACS Nano **5**, 6586 (2011).
[28] S. Mühlig, C. Rockstuhl, V. Yannopapas, T. Bürgi, N. Shalkevich, and F. Lederer, Opt. Express **19**, 9607 (2011).
[29] L. Malassis, P. Massé, M. Tréguer-Delapierre, S. Mornet, P. Weisbecker, V. Kravets, A. Grigorenko, and P. Barois, Langmuir **29**, 1551 (2013).
[30] W. Park, K. Emoto, Y. Jin, A. Shimizu, V. A. Tamma, and W. Zhang, Opt. Mater. Exp. **3**, 205 (2013).
[31] C. Rockstuhl, C. Menzel, S. Mühlig, J. Petschulat, C. Helgert, C. Etrich, A. Chipouline, T. Pertsch, and F. Lederer, Phys. Rev. B **83**, 245119 (2011).
[32] M. Fruhnert, S. Mühlig, F. Lederer, and C. Rockstuhl, Phys. Rev. B **89**, 075408 (2014).
[33] B. Hopkins, A. N. Poddubny, A. E. Miroshnichenko, and Y. S. Kivshar, Phys. Rev. A **88**, 053819 (2013).
[34] B. Hopkins, D. S. Filonov, A. E. Miroshnichenko, F. Monticone, A. Alù, and Y. S. Kivshar, ACS Photon. **2**, 724 (2015).
[35] D. A. Bykov and L. L. Doskolovich, J. Lightwave Technol. **31**, 793 (2013).
[36] C. Sauvan, J. P. Hugonin, I. S. Maksymov, and P. Lalanne, Phys. Rev. Lett. **110**, 237401 (2013).
[37] F. Alpeggiani, N. Parappurath, E. Verhagen, and L. Kuipers, Phys. Rev. X **7**, 021035 (2017).
[38] B. Vial and Y. Hao, J. Opt. **18**, 115004 (2016).
[39] R. N. S. Suryadharma, A. A. Iskandar, and M.-O. Tjia, J. Appl. Phys. **120**, 043105 (2016).
[40] X. Zheng, V. Volskiy, V. K. Valev, G. A. E. Vandenbosch, and V. V. Moshchalkov, IEEE J. Sel. Top. Quantum Electron. **19**, 4600908 (2013).
[41] X. Zheng, N. Verellen, V. Volskiy, V. K. Valev, J. J. Baumberg, G. A. E. Vandenbosch, and V. V. Moshchalkov, Opt. Express **21**, 31105 (2013).
[42] I. P. Kovalyov and D. M. Ponomarev, IEEE Trans. Antennas Propag. **59**, 4181 (2011).
[43] M. S. Khajeahsani, A. Shahmansouri, M. J. Armand, and B. Rashidian, J. Opt. Soc. Am. B **32**, 2333 (2015).
[44] J. Jackson, *Classical Electrodynamics* (Wiley, New York, 1998).
[45] G. Gouesbet, Opt. Commun. **283**, 517 (2010).
[46] M. Fruhnert, A. Monti, I. Fernandez-Corbaton, A. Alù, A. Toscano, F. Bilotti, and C. Rockstuhl, Phys. Rev. B **93**, 245127 (2016).
[47] J.-C. Auger and B. Stout, J. Quant. Spectrosc. Radiat. Transfer **79**, 533 (2003).

[48] S. Stein, Q. Appl. Math. **19**, 15 (1961).
[49] Y. lin Xu, Appl. Opt. **34**, 4573 (1995).
[50] V. Myroshnychenko, J. Rodriguez-Fernandez, I. Pastoriza-Santos, A. M. Funston, C. Novo, P. Mulvaney, L. M. Liz-Marzan, and F. J. Garcia de Abajo, Chem. Soc. Rev. **37**, 1792 (2008).
[51] C. R. Simovski and S. A. Tretyakov, Phys. Rev. B **79**, 045111 (2009).
[52] S. N. Sheikholeslami, H. Alaeian, A. L. Koh, and J. A. Dionne, Nano Lett. **13**, 4137 (2013).
[53] D. W. Mackowski and M. I. Mishchenko, J. Opt. Soc. Am. A **13**, 2266 (1996).
[54] A. Sihvola, Progress Electromagn. Res. **62**, 317 (2006).
[55] C. Helgert, C. Rockstuhl, C. Etrich, C. Menzel, E.-B. Kley, A. Tünnermann, F. Lederer, and T. Pertsch, Phys. Rev. B **79**, 233107 (2009).
[56] M. Albooyeh, S. Kruk, C. Menzel, C. Helgert, M. Kroll, A. Krysinski, M. Decker, D. N. Neshev, T. Pertsch, C. Etrich, C. Rockstuhl, S. A. Tretyakov, C. R. Simovski, and Y. S. Kivshar, Sci. Rep. **4**, 4484 (2014).